

Complete one-loop corrections to $e^+e^- \rightarrow W^+W^-$ in the MSSM

T. Hahn

Institut für Theoretische Physik, Universität Karlsruhe
D-76128 Karlsruhe, Germany

July 7, 2000

Abstract

The complete $\mathcal{O}(\alpha_s)$ corrections including soft-photon bremsstrahlung to the process $e^+e^- \rightarrow W^+W^-$ in the MSSM are calculated for on-shell W bosons. The difference between the Standard Model and MSSM one-loop corrections is less than 2.7% over the scanned parameter space.

1 Introduction

The process $e^+e^- \rightarrow W^+W^-$ is already one of the key processes at LEP2, and will be of similar importance at future linear e^+e^- colliders. Hence it is not surprising that considerable theoretical effort has gone into the precise prediction of the cross-section in the Standard Model (SM), both for on- and off-shell W bosons (see [1] and references therein).

For a process well accessible both experimentally and theoretically in the SM, one of the obvious questions to ask is whether it can tell us anything about physics beyond the SM. Supersymmetric extensions play a special role because they, like the SM, allow to make precise predictions in terms of a set of input parameters. Previous calculations in supersymmetric theories include the complete one-loop corrections in spontaneously broken supersymmetry [2] and sfermion-loop effects in the MSSM [3].

In this paper the complete one-loop corrections for $e^+e^- \rightarrow W^+W^-$ in the MSSM including real bremsstrahlung in the soft-photon approximation are presented. The results are rather small: the maximum deviation from the SM value within the scanned parameter space is 2.7%.

The outline of this paper is as follows. In Sect. 2 the kinematics and notation are fixed. Sect. 3 describes the details of the one-loop calculation. The results of the calculation and the scan over the MSSM parameter space are presented in Sect. 4. Sect. 5 finally gives the conclusions.

2 Kinematics and notation

The reaction studied here is

$$e^+(k_1; \lambda_1) + e^-(k_2; \lambda_2) \rightarrow W^+(k_3; \lambda_3) + W^-(k_4; \lambda_4); \quad (1)$$

where k_i and λ_i represent the momenta and helicities of the external particles, respectively.

The incoming particles travel along the z axis and are scattered into the $x\{z$ plane. Neglecting the electron mass, the explicit representations of the momenta and the polarization vectors in the centre-of-mass system are

$$\begin{aligned} k_1 &= E(1; 0; 0; -1); & \epsilon_3^i(0) &= (p; E \sin \theta; 0; E \cos \theta) = M_W \epsilon^i; \\ k_2 &= E(1; 0; 0; 1); & \epsilon_3^i(\theta) &= (0; \cos \theta; i; \sin \theta) = \frac{p}{\sqrt{2}} \epsilon^i; \\ k_3 &= (E; p \sin \theta; 0; p \cos \theta); & \epsilon_4^i(0) &= (p; -E \sin \theta; 0; E \cos \theta) = M_W \epsilon^i; \\ k_4 &= (E; p \sin \theta; 0; -p \cos \theta); & \epsilon_4^i(\theta) &= (0; \cos \theta; -i; \sin \theta) = \frac{p}{\sqrt{2}} \epsilon^i; \end{aligned} \quad (2)$$

where ϵ^i is the velocity of the electrons, $p = \frac{p}{E^2 - M_W^2}$ is the momentum of the W bosons, $E = \frac{p}{\sqrt{2}}$ is the beam energy, and θ is the scattering angle.

The polarized differential cross-section is obtained from the helicity amplitudes $M_{\lambda_1 \lambda_2 \lambda_3 \lambda_4}$ as

$$\frac{d}{d\cos\theta} \sigma_{\lambda_1 \lambda_2 \lambda_3 \lambda_4} = \frac{1}{64\pi^2 s} |M_{\lambda_1 \lambda_2 \lambda_3 \lambda_4}|^2; \quad (3)$$

In the following, only unpolarized electrons are considered, since that is the situation at LEP 2. In this case the cross-section has to be averaged over the initial helicities according to

$$\frac{d}{d\cos\theta} \sigma_{UU} = \frac{1}{4} \sum_{\lambda_1, \lambda_2 = \pm 1} \frac{d}{d\cos\theta} \sigma_{\lambda_1 \lambda_2 \lambda_3 \lambda_4}; \quad (4)$$

Polarization combinations are given by a sequence of four letters, e.g. $UU\bar{L}\bar{T}$, where L, T , and U denote longitudinal ($\lambda = 0$), transverse ($\lambda = \pm 1$), and unpolarized particles.

3 One-loop corrections

Since the coupling of the electron to any of the Higgs particles in the SM or the MSSM is suppressed by a factor m_e/M_W , the Higgs-exchange diagrams can safely be neglected. The tree-level diagrams are then the same for the SM and the MSSM, i.e. γ and Z exchange in the s -channel and neutrino exchange in the t -channel (see Fig. 1). The tree-level results shall not be discussed here as this has been done in detail elsewhere [1].

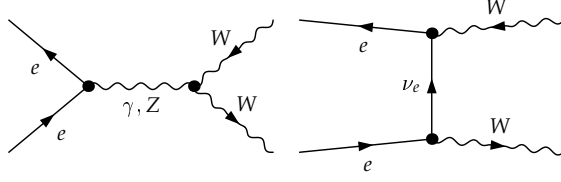


Figure 1: The tree-level diagrams.

3.1 Computational framework

The calculation of the $\mathcal{O}(\alpha^2)$ radiative corrections has been performed in 't Hooft-Feynman gauge. Ultraviolet (UV) divergences are treated within dimensional regularization. For the renormalization the on-shell scheme [4] is used, following the formulation worked out in [5]. In the absence of SUSY particles at tree level, only those counter-terms appear that are already present in the SM. The only change is that now the selfenergies from which the renormalization constants are derived have to be calculated in the MSSM.

To $\mathcal{O}(\alpha^2)$, the squared matrix element is given by

$$|\mathcal{M}|^2 = |\mathcal{M}_{\text{Bom}}|^2 (1 + \delta_{\text{soft}}) + 2 \text{Re}(\mathcal{M}_{\text{Bom}} \mathcal{M}_{\text{1-loop}}) ; \quad (5)$$

where \mathcal{M}_{Bom} and $\mathcal{M}_{\text{1-loop}}$ denote the sum of the contributing tree-level and one-loop Feynman diagrams, respectively, and δ_{soft} is the QED correction factor from realbremsstrahlung in the soft-photon approximation.

The Feynman diagrams are generated with FeynArts [6] which in its current version uses algorithms that can deal with supersymmetric theories [7]. The resulting amplitudes are algebraically simplified using FormCalc [8, 9] and then converted to a Fortran program. For evaluating the one-loop scalar and tensor integrals the LoopTools package [8, 10] is used. The SM results of [1] were fully confirmed with this method.

3.2 QED corrections

In addition to the virtual diagrams, realphoton emission from the external legs has to be taken into account to cancel the infrared (IR) divergences which arise from the exchange of massless photons. The IR divergences are regularized by an infinitesimal photon mass k_0 . In the soft-photon limit the cross-section for realphoton emission is proportional to the Bom cross-section,

$$\frac{d}{d\Omega} \bigg|_{\text{soft}} = \frac{d}{d\Omega} \bigg|_{\text{Bom}} \delta_{\text{soft}} ; \quad (6)$$

with the soft-photon factor δ_{soft} given by

$$\delta_{\text{soft}} = \frac{e^2}{(2\pi)^3} \int_{k_0 \leq E} \frac{d^3k}{2k_0} \sum_{i,j=1}^4 \frac{Q_i Q_j (k_i k_j)}{(k_i k) (k_j k)} \bigg|_{k_0 = \frac{P}{k^2 + \epsilon^2}} ; \quad (7)$$

Here E is the maximum energy of the emitted photons, Q_i is the charge of the i th external particle, and the sign in front of the product $Q_i Q_j$ is + if particles i and j are both either incoming or outgoing, and otherwise. The basic integrals needed for the evaluation of (7) have been worked out e.g. in [11].

The absolute magnitude of the $O(\alpha_s)$ corrections is largely determined by the QED contributions and depends strongly on the photon-energy cutoff E through logarithms of the form $\log E = E$. Without an experimentally motivated choice of E , the overall size of the one-loop corrections can be shifted more or less at will using different values of E . Since the intention here is only to show the differences between the SM and the MSSM calculations, the concrete value of E is rather unimportant. Hard-photon radiation is omitted in the present calculation since it can be taken over directly from the SM calculation.

In this calculation a soft-photon cutoff energy of $E = 0.05 \sqrt{s}$ is used as in [1].

3.3 Inventory of one-loop diagrams

This section lists the contributing one-loop diagrams. The diagrams can be separated into selfenergy contributions, vertex corrections, and box corrections. Note that diagrams which are already present in the SM are omitted in the figures.

The selfenergy contributions fall into two categories, corrections to the γ and Z propagator in the s -channel, and corrections to the γ propagator in the t -channel. These diagrams are shown in Fig. 2.

The vertex diagrams can be grouped into corrections to the initial- and final-state vertex in the s -channel (Figs. 3 and 4), and corrections to the t -channel vertices (Fig. 5).

Finally, the box diagrams are displayed in Fig. 6.

4 Numerical results

4.1 Input parameters

4.1.1 Standard Model parameters

For the SM parameters the following numerical values are used:

$$\begin{aligned}
 \alpha_s^1 &= 137.0359895; & M_Z &= 91.1867 \text{ GeV}; & M_W &= 80.39 \text{ GeV}; \\
 m_e &= 0.51099907 \text{ MeV}; & m_u &= 53.8 \text{ MeV}; & m_d &= 53.8 \text{ MeV}; \\
 m_c &= 105.658389 \text{ MeV}; & m_c &= 1.50 \text{ GeV}; & m_s &= 150 \text{ MeV}; \\
 m_b &= 1777 \text{ MeV}; & m_t &= 174 \text{ GeV}; & m_b &= 4.7 \text{ GeV};
 \end{aligned} \tag{8}$$

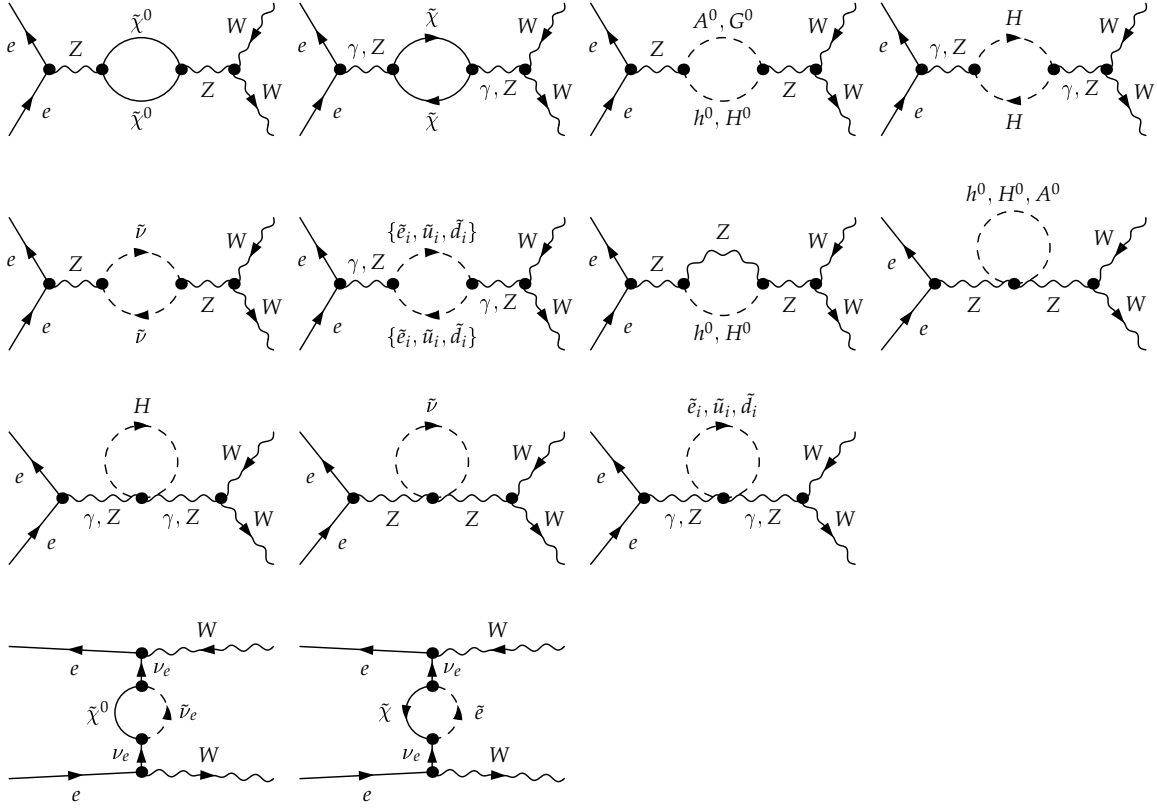


Figure 2: The M SSM self-energy corrections. Braces indicate that there is one diagram for the first members of all braced lists, one for the second members, etc. A sfermion with index i accounts for six particles, e.g. $\mathbf{e}_1 = \{e^1; e^2; \tilde{e}^1; \tilde{e}^2; \tilde{e}^1; \tilde{e}^2\}$.

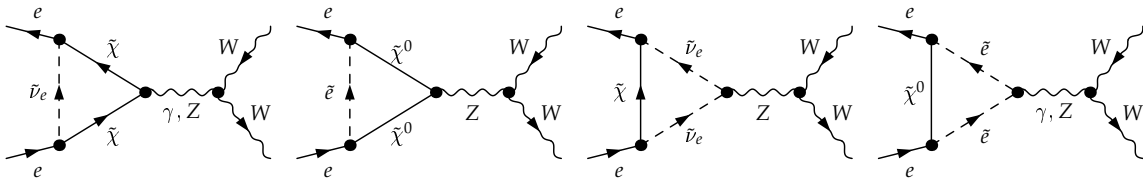


Figure 3: The M SSM contributions to the initial-state vertex in the s-channel.

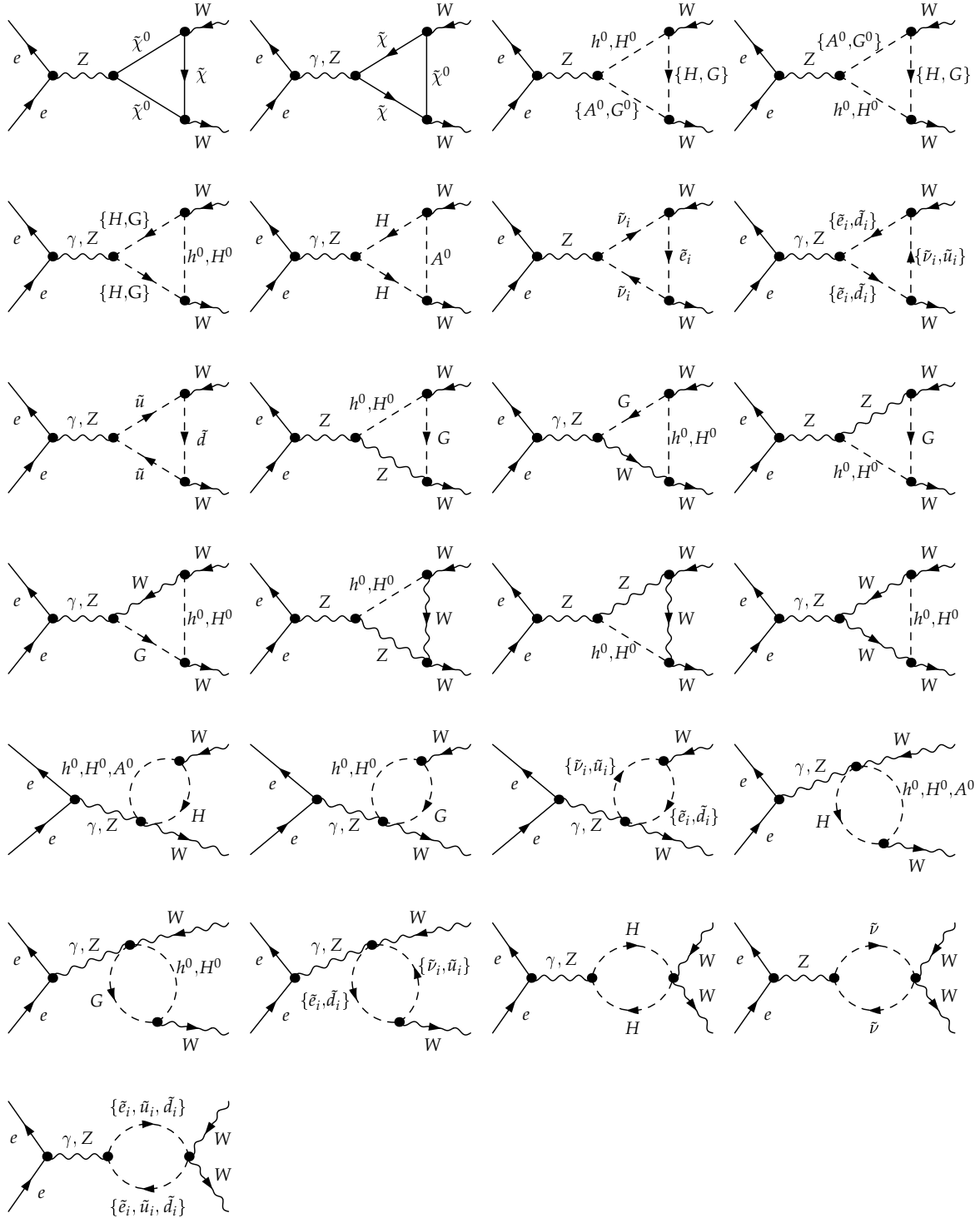


Figure 4: TheM SSM contributions to the s-channel neutral-state vertex. Braces indicate that there is one diagram for the first members of all braced lists, one for the second members, etc. A sfermion with index i accounts for six particles, e.g. $e_i = \{e^1; e^2; \tilde{e}^1; \tilde{e}^2; \tilde{e}^1; \tilde{e}^2\}g$.

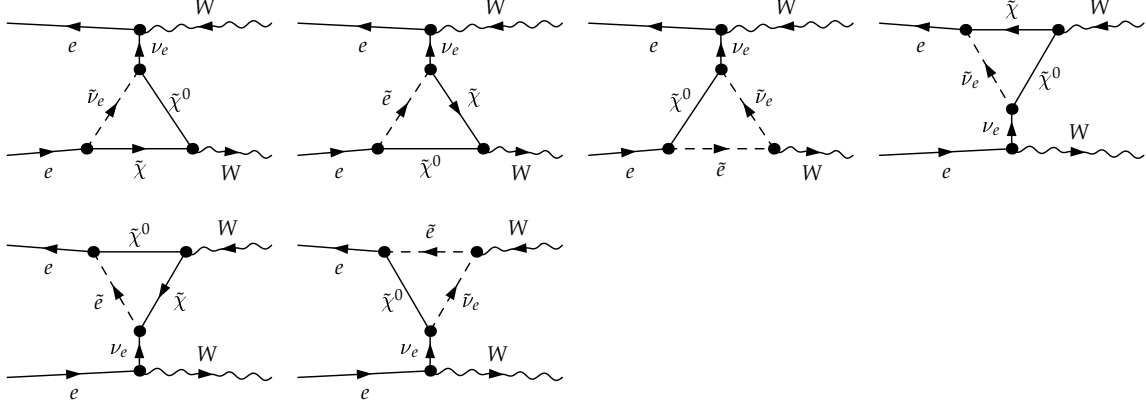


Figure 5: The M SSM contributions to the t-channel vertices.

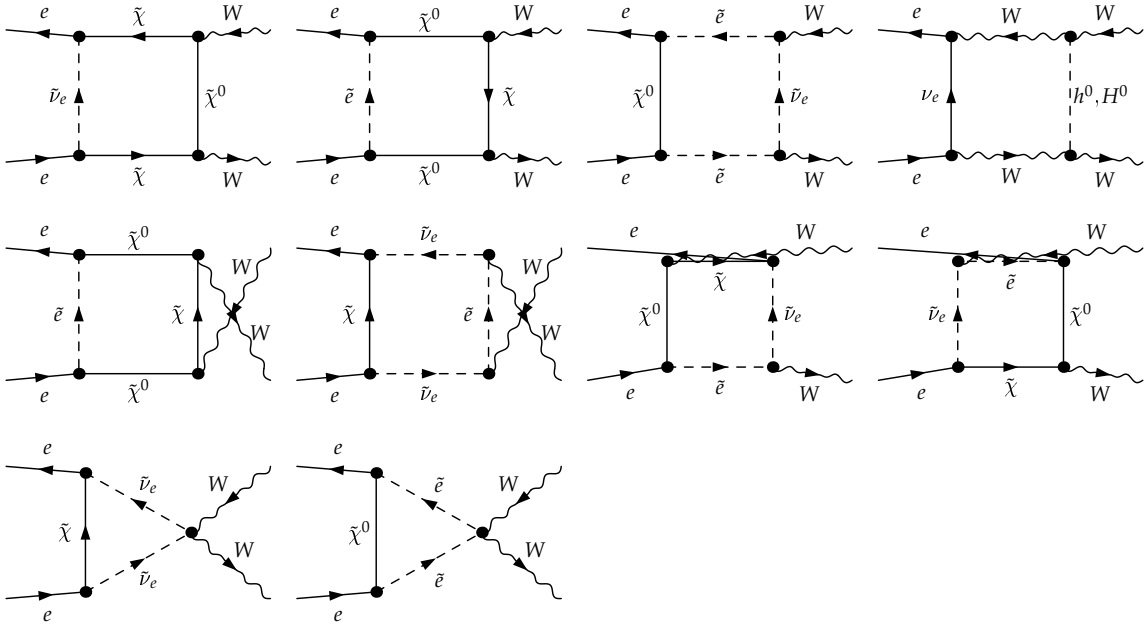


Figure 6: The M SSM box diagrams.

The masses of the up and down quarks are effective parameters which are adjusted such that the vector hadronic contribution to a_μ is 0.02778 [12], i.e.

$$\alpha_{\text{had}}^{(5)}(s = M_Z^2) = - \sum_{f=u,d,s,b} Q_f^2 \log \frac{M_Z^2}{m_f^2} \frac{5}{3} \stackrel{!}{=} 0.02778 :$$

4.1.2 MSSM parameters

Higgs sector The neutral Higgs sector is fixed by choosing a value for $\tan \beta$ and for the mass M_{A^0} of the CP-odd neutral Higgs boson A^0 . For the other neutral Higgs masses which receive significant radiative corrections the two-loop approximation formula of [13] is used.

There are only small radiative corrections for the charged Higgs masses and the following equation holds for $M_{A^0} \gg O(M_W)$ [14].

$$M_H^2 = M_{A^0}^2 + M_W^2 + \frac{5 M_W^2}{2 C_W^2} \ln \frac{M_{\text{SUSY}}}{M_W} + \frac{3}{4 S_W^2 M_W^2} \frac{2 m_{tr}^2 m_b^2}{\sin^2 \cos^2} M_W^2 \frac{m_{tr}^2}{\sin^2} + \frac{m_b^2}{\cos^2} + \frac{2}{3} M_W^4 \ln \frac{M_{\text{SUSY}}}{m_{tr}} ; \quad (9)$$

where M_{SUSY} is a universal soft-SUSY-breaking mass introduced in the next paragraph and $m_{tr} = m_t (1 + 4 s_s(m_t) = 3)^{-1}$ is the running top mass.

Sfermions For simplicity, all soft-SUSY-breaking parameters are assumed equal and mixing between sfermion generations is neglected, so that

$$M_Q^2 = M_U^2 = M_D^2 = M_L^2 = M_E^2 = M_{\text{SUSY}}^2 \mathbb{1}; \\ A_U = A_u \mathbb{1}; \quad A_L = A_D = A_d \mathbb{1}; \quad (10)$$

Then, the sfermion mass matrix is given by [15, 16]

$$M_{\text{SUSY}}^2 + M_Z^2 \cos(2\beta) (I_3^f - Q_f S_W^2) + m_f^2 \frac{(A_{fudg} - f_{\text{foot}} \tan \beta)}{m_f (A_{fudg} - f_{\text{foot}} \tan \beta)} M_{\text{SUSY}}^2 + M_Z^2 \cos(2\beta) Q_f S_W^2 + m_f^2 \quad (11)$$

where the elements in braces apply to $I_3^f = +\frac{1}{2}$ and $-\frac{1}{2}$, respectively.

Charginos and Neutralinos The chargino mass matrix [15, 16]

$$X = \begin{pmatrix} M_2 & \sqrt{2} M_W \sin \beta \\ \sqrt{2} M_W \cos \beta & M_1 \end{pmatrix} \quad (12)$$

and the neutralino mass matrix [15, 16]

$$Y = \begin{pmatrix} 0 & M_1 & 0 & M_Z s_W \cos & M_Z s_W \sin & 1 \\ B & 0 & M_2 & M_Z c_W \cos & M_Z c_W \sin & C \\ B & M_Z s_W \cos & M_Z c_W \cos & 0 & 0 & C \\ 0 & M_Z s_W \sin & M_Z c_W \sin & 0 & 0 & A \end{pmatrix} \quad (13)$$

are diagonalized with unitary matrices U , V , and N such that

$$\begin{aligned} U X V^{-1} &= \text{diag}(m_{\tilde{\chi}_1}, m_{\tilde{\chi}_2}); \\ N Y N^{-1} &= \text{diag}(m_{\tilde{\chi}_1^0}, \dots, m_{\tilde{\chi}_4^0}); \end{aligned} \quad (14)$$

This diagonalization is done numerically using the subroutines of the LAPACK library [17]. The $U(1)$ gaugino-mass parameter M_1 which appears as a further input parameter in Y is fixed, as usual, by the $SUSY-GUT$ relation

$$M_1 = \frac{5s_W^2}{3c_W^2} M_2; \quad (15)$$

4.1.3 Parameter scan

The remaining input parameters are then scanned over the following regions:

SM	MSSM	
$M_H = 100 :: 300 \text{ GeV}$	$\tan \beta = 1.5; 5; 50$ $M_{A^0} = 100 :: 1000 \text{ GeV}$ $\phantom{M_{A^0}} = 1000 :: 1000 \text{ GeV}$ $M_2 = 100 :: 1000 \text{ GeV}$ $M_{SUSY} = 100 :: 1000 \text{ GeV}$ $A_u = A_d = M_{SUSY}; 2M_{SUSY}$	(16)

When the particle masses are calculated from these input parameters, the Fortran program checks whether they are consistent with the current exclusion limits and automatically omits already-excluded points in parameter space from the scan. The following bounds are used:

$$\begin{aligned} M_{\tilde{t}} &> 80 \text{ GeV} \quad [18]; & M_{h^0} &> 85 \text{ GeV} \quad [20]; \\ M_{\tilde{g}} &> 70 \text{ GeV} \quad [18]; & m_{\tilde{\chi}_1^0} &> 30 \text{ GeV} \quad [21]; \\ M_{\tilde{q}, \tilde{b}, \tilde{\tau}} &> 150 \text{ GeV} \quad [18]; & m_{\tilde{\chi}_2^0} &> 90 \text{ GeV} \quad [21]; \\ M_{\tilde{\nu}_\tau} &> 70 \text{ GeV} \quad [19]; \end{aligned} \quad (17)$$

4.2 Results

In Fig. 7 the absolute values of the total and differential cross-section in the SM and MSSM is shown for three different polarizations: UUUU (all particles unpolarized), UUTT

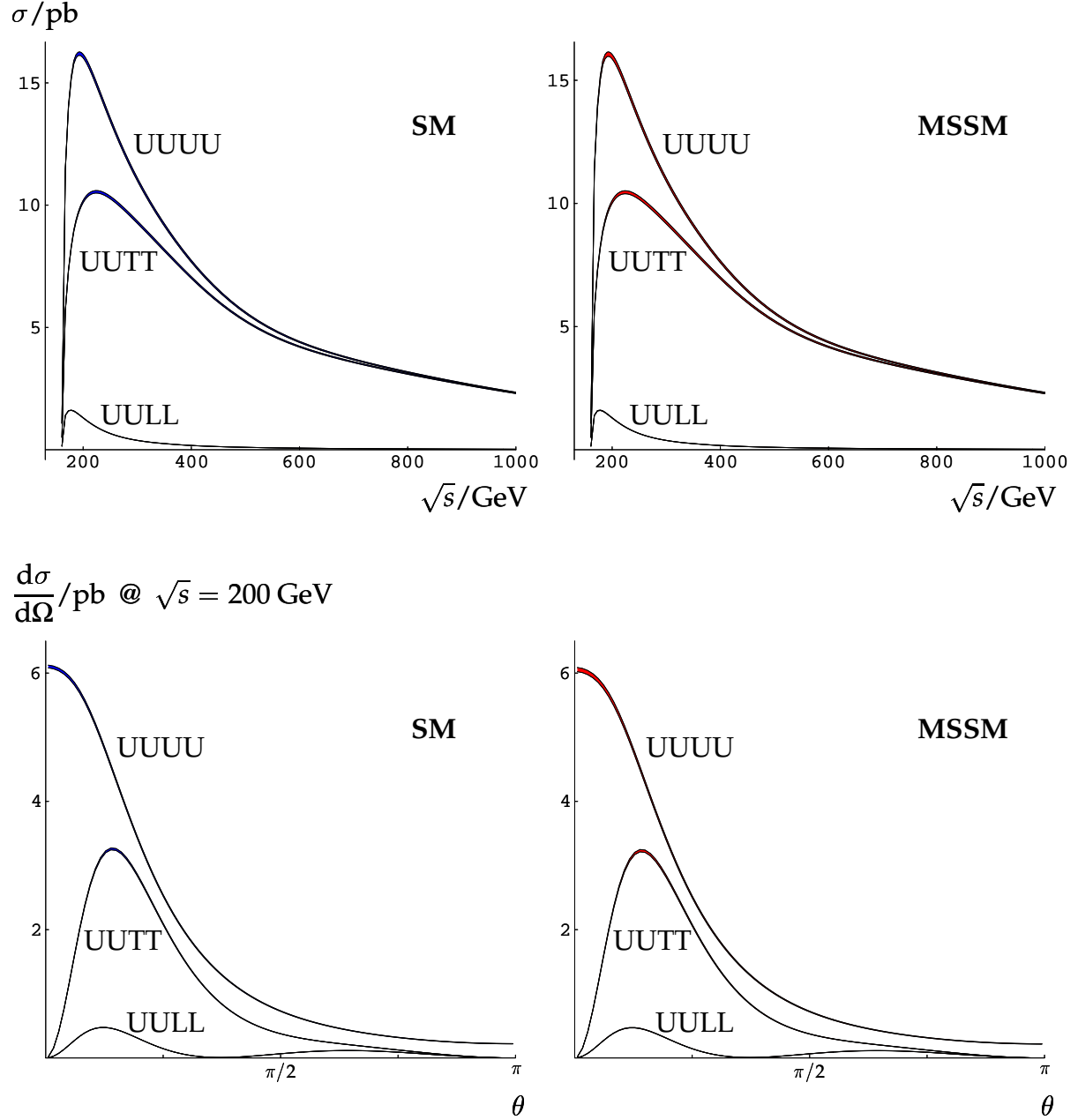


Figure 7: The total cross-section and the differential cross-section at $\sqrt{s} = 200 \text{ GeV}$ for the SM and the MSSM. The thickness of the curves give the range of allowed values within the parameter scan (16).

(transverse W bosons), and $UU LL$ (longitudinal W bosons). The thickness of the curves reflects the range of the allowed values within the parameter scan (16).

Fig. 8 shows the relative corrections in the SM and MSSM with respect to the Born cross-section. The overall magnitude of the corrections is largely determined by the well-understood QED logarithms, as discussed in Sect. 3.2. The bands show the variation of the cross-section within the parameter scan (16). Characteristically, the bands for the SM and MSSM overlap slightly, the MSSM band being the lower one. The two bands are of comparable width of the order of a few percent for all polarizations. The dominating polarizations over the entire energy range are UU , and this explains why the plots for the $UUUU$ and $UUTT$ polarizations in Fig. 8 are quite similar.

The relative deviation between the SM central value and the MSSM band is plotted in Fig. 9. While the largest corrections (2.7% at 1 TeV) are seen for purely longitudinal W bosons, one has to keep in mind that the cross-section for longitudinally polarized W bosons is much smaller than for the transverse polarizations. In the transverse polarizations and in the unpolarized case the maximum deviation between the SM and the MSSM is roughly 1.5%. The maximum deviation is reached in all polarizations for light SUSY particles, for example in the unpolarized case ($UUUU$) the lightest higgs, stop, chargino, and neutralino masses at the point of maximum deviation are $M_{h^0} = 91$ GeV, $M_{\tilde{t}} = 165$ GeV, $m_{\tilde{\chi}^\pm} = 117$ GeV, and $m_{\tilde{\chi}^0} = 52$ GeV, respectively.

Finally, the variation of the cross-section with the scanned MSSM parameters is shown in Fig. 10. The largest variation is connected with the soft-SUSY-breaking mass M_{SUSY} and confirms the idea of the previous calculation [3] that important contributions come from the sfermion sector. Nevertheless, the contributions from the other sectors are similar in size and cannot be neglected.

5 Conclusions

The MSSM corrections to $e^+e^- \rightarrow W^+W^-$ are probably too small to be detected at LEP 2, taking into account that the convolution with decay amplitudes in the final and photon radiation in the initial state tends to smear the corrections.

With the projected accuracy of a linear collider, however, corrections of this magnitude will play a role. Although the calculation presented here is limited to on-shell W bosons and hard-bremsstrahlung effects have not been considered, these effects are the same for the SM and the MSSM, hence it should be possible to use the MSSM cross-section presented here in a straightforward way in existing Monte Carlo generators, for example [22].

Acknowledgements

I thank W. Hollik for discussions, C. Schappacher for help with the implementation of the MSSM parameter scan in Fortran, and G. Weiglein for proofreading the manuscript.

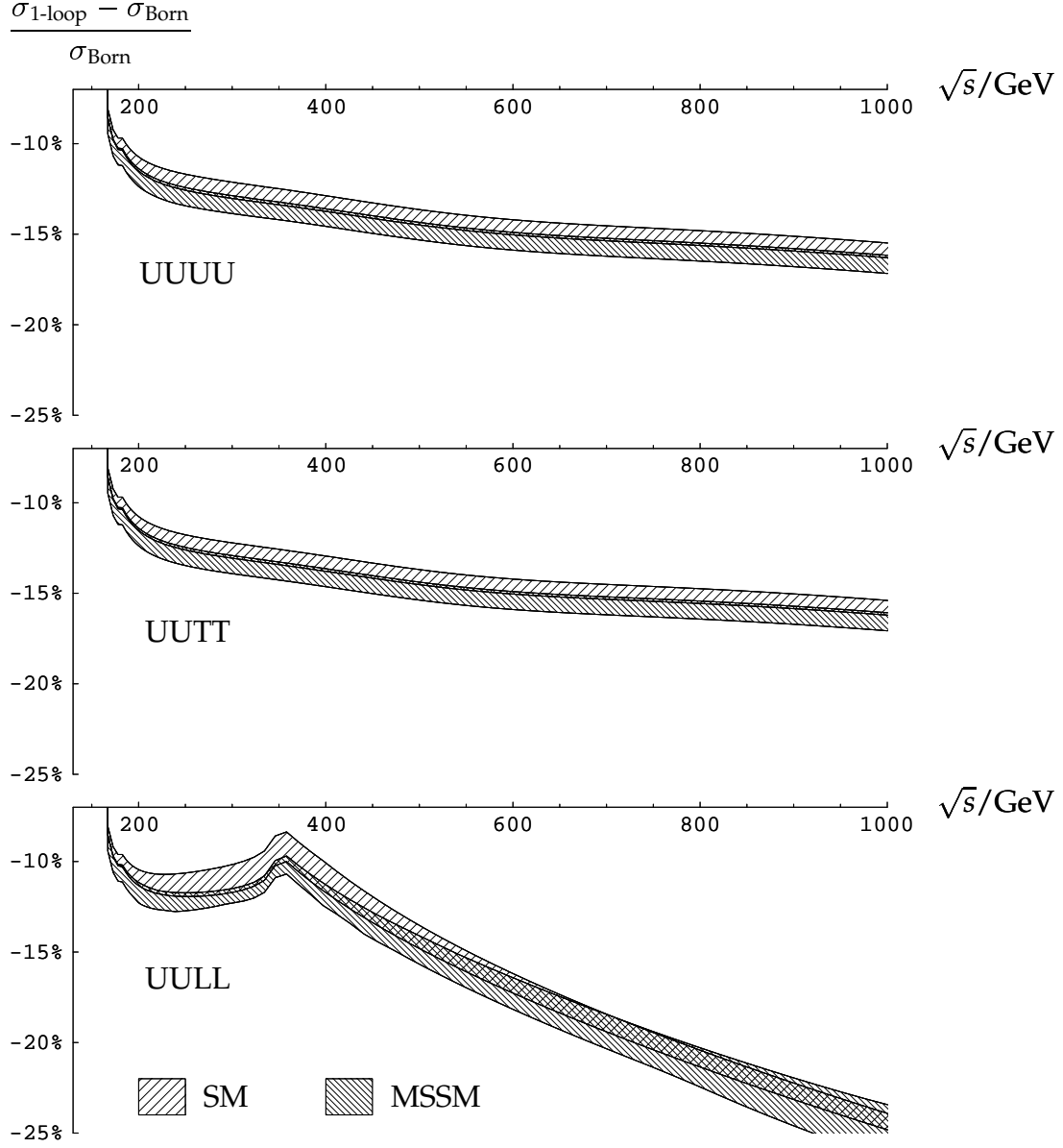


Figure 8: The relative difference between the one-loop corrected and the Born cross-section. The cross-hatched bands indicate the minimum and maximum reached within the scan over the parameter space (16).

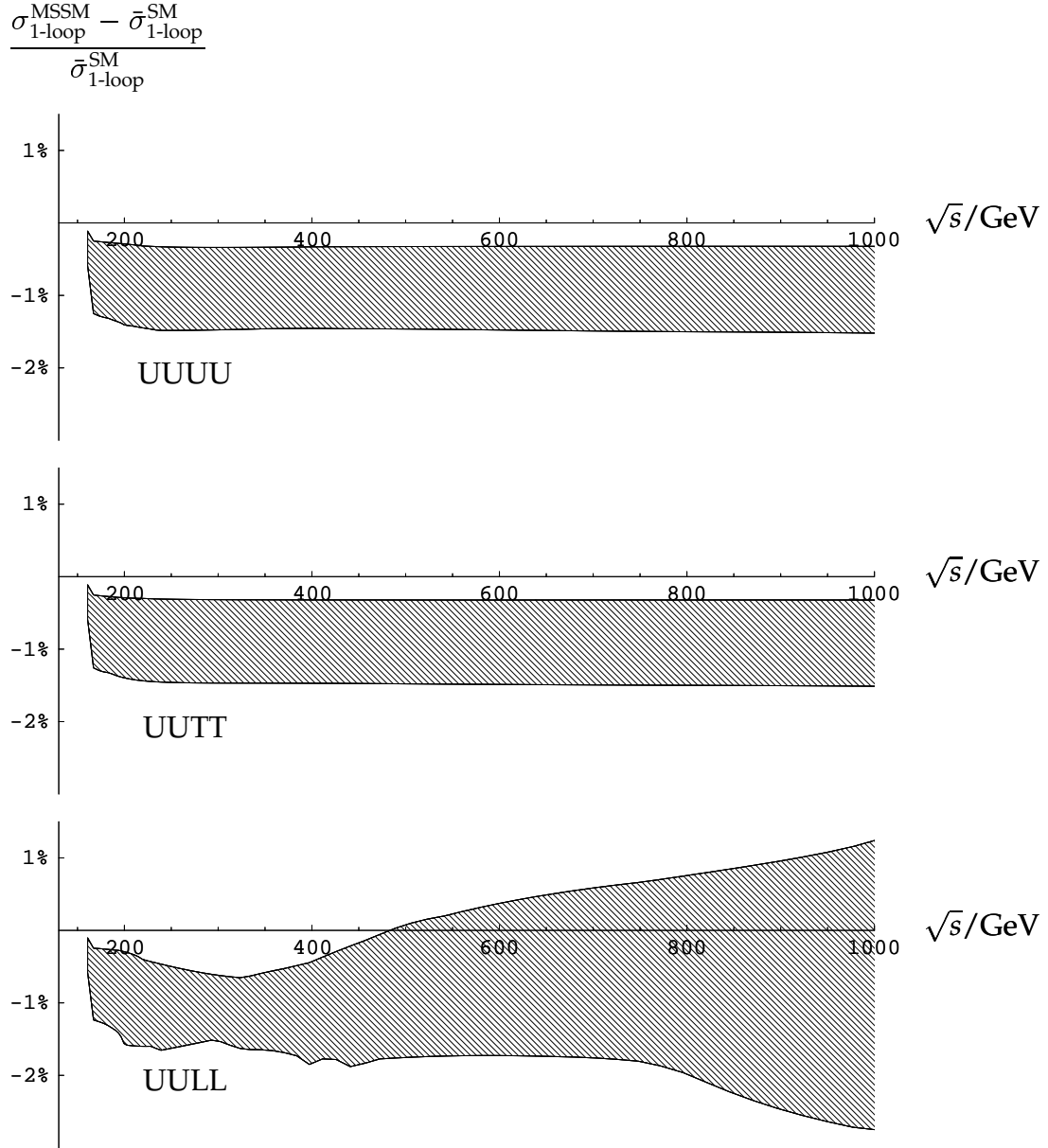


Figure 9: The relative difference between the SM central value $\bar{\sigma}_{1\text{-loop}}^{\text{SM}}$ and the MSSM bands of Fig. 8.

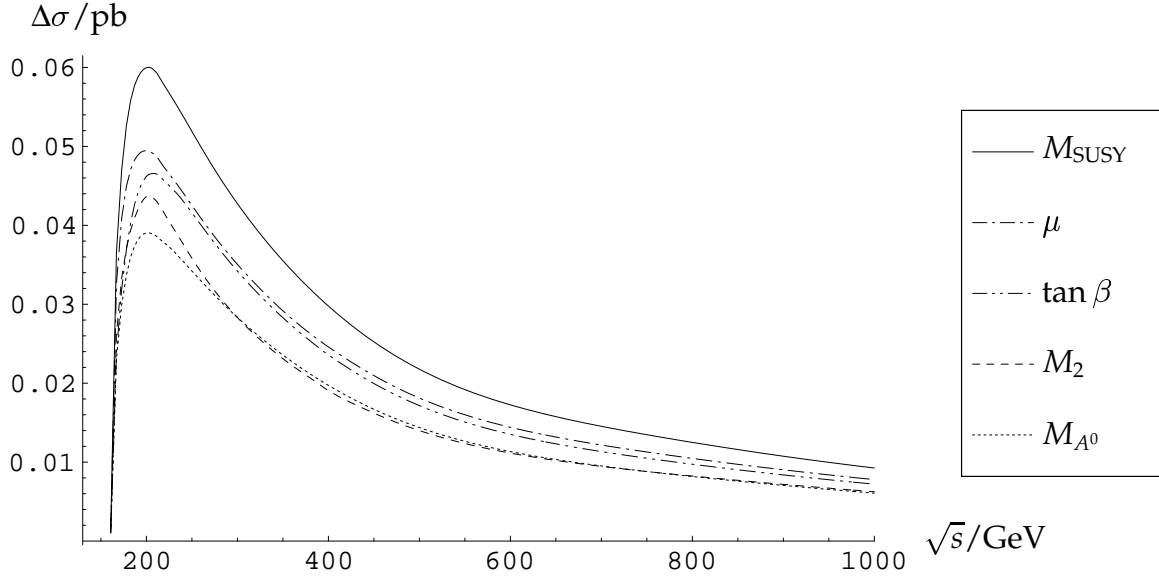


Figure 10: The variation of the MSSM cross-section for unpolarized particles with the scanned MSSM parameters. The variation of a parameter X is computed as the difference between maximum and minimum of the cross-section for fixed X , averaged over all values of X .

Parts of this calculation have been performed on the QCM computer cluster at the University of Karlsruhe, supported by the Deutsche Forschungsgemeinschaft (Forschergruppe \Quantenfeldtheorie, Computeralgebra und Monte-Carlo Simulation").

References

- [1] W. Beenakker and A. Denner, Int. J. Mod. Phys. A 9 (1994) 4837.
- [2] S. Alam, Phys. Rev. D 50 (1994) 124, 148, 174.
- [3] S. Alam, K. Hagiwara, S. Kanemura, R. Szalapski, and Y. Ueda, hep{ph/0002066.
- [4] D. A. Ross and J. C. Taylor, Nucl. Phys. B 51 (73) 125, E Nucl. Phys. B 58 (1973) 643;
A. Sirlin, Phys. Rev. D 22 (1980) 971;
K. I. Aoki et al., Suppl. Prog. Theor. Phys. 73 (1982) 1;
M. Bohm, W. Hollik, and H. Spiesberger, Fortschr. Phys. 34 (1986) 687.
- [5] A. Denner, Fortschr. Phys. 41 (1993) 307.
- [6] J. Kublbeck, M. Bohm and A. Denner, Comp. Phys. Commun. 60 (1991) 165;
T. Hahn, FeynArts 2.2 user's guide, available from <http://www.feynarts.de>.

- [7] T. Hahn, [hep{ph/0005029](#).
- [8] T. Hahn and M. Perez-Victoria, *Comp. Phys. Commun.* **118** (1999) 153.
- [9] T. Hahn, FormCalc user's guide, available from <http://www.feynarts.de/formcalc>.
- [10] T. Hahn, LoopTools user's guide, available from <http://www.feynarts.de/looptools>.
- [11] G. 't Hooft and M. Veltman, *Nucl. Phys. B* **410** (1993) 245.
- [12] F. Jegerlehner, [hep{ph/9901386](#).
- [13] S. Heinemeyer, W. Hollik, and G. Weiglein, *Phys. Lett. B* **455** (1999) 179.
- [14] M. A. Diaz, Radiative Corrections to Higgs Masses in the Minimal Supersymmetric Model, Ph.D. Thesis, June 1992, Univ. of California (Santa Cruz), SCIPP-92-13.
- [15] H. E. Haber and G. Kane, *Phys. Rep.* **117** (1985) 75.
- [16] J. F. Gunion and H. E. Haber, *Nucl. Phys. B* **272** (1986) 1.
- [17] E. Anderson et al., LAPACK user's guide, SIAM Press, Philadelphia (1999), ISBN 0898714478.
- [18] L3 Collaboration, *Phys. Lett. B* **471** (1999) 308.
- [19] L3 Collaboration, *Phys. Lett. B* **471** (1999) 280.
- [20] ALEPH Collaboration, [hep{ex/9908016](#).
- [21] L3 Collaboration, *Phys. Lett. B* **472** (2000) 420;
OPAL Collaboration, [hep{ex/9909051](#).
- [22] A. Denner, S. Dittmaier, M. Roth, and D. Wackeroth, [hep{ph/0006307](#).